

Geometry-aware Compensation Scheme for Morphing Drones

Amedeo Fabris, Kevin Kleber, Davide Falanga and Davide Scaramuzza

Abstract—Morphing multirotors, such as the Foldable Drone [1], can increase the versatility of drones employing in-flight-adaptive-morphology. To further increase precision in their tasks, recent works have investigated stable flight in asymmetric morphologies mainly leveraging the low-level controller. However, the aerodynamic effects embedded in multirotors are only analyzed in fixed shape aerial vehicles and are completely ignored in morphing drones. In this paper, we investigate the effects of the partial overlap between the propellers and the main body of a morphing quadrotor. We perform experiments to characterize such effects and design a morphology-aware control scheme to account for them. To guarantee the right trade-off between efficiency and compactness of the vehicle, we propose a simple geometry-aware compensation scheme based on the results of these experiments. We demonstrate the effectiveness of our approach by deploying the compensation scheme on the Foldable Drone, a quadrotor that can fold its arms around the main body. The same set of experiments is performed and compared against one another by activating and deactivating the compensation scheme offline or during the flight. To the best of our knowledge, this is the first work counteracting the aerodynamic effects of a morphing quadrotor during flight and showing the effects of partial overlap between a propeller and the central body of the drone.

SUPPLEMENTARY MATERIAL

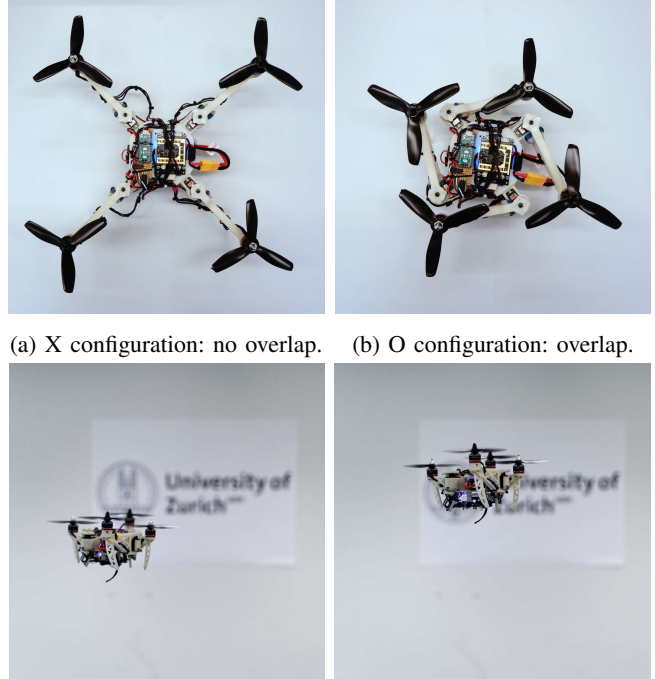
All the videos of the experiments are available at:
<https://youtu.be/Na0yrkCsC-M>

I. INTRODUCTION

In recent years, adaptive morphology [1], [2], [3], [4], [5], [6] has increased the already ubiquitous use of multirotors [7]. This key advancement in autonomous drones has led to increased versatility in applications, such as delivery, proximity inspections, and search and rescue [8], [9].

The higher maneuverability of morphing drones compared to standard fixed-shape drones in challenging scenarios is achieved without miniaturizing the drone, thus with consequent benefits in terms of flight time, payload, and robustness to air perturbations. Yet, most of the current morphing platforms [2], [3], [4], [5], [6] are either designed to perform single tasks, completely rely on the effort of the low level controller, or are based on passive flight. The works in [2], [6], [3] present morphing quadrotors with different designs, but similar limitations: all the presented aerial vehicles can traverse vertical gaps, but while only the last one guarantees continuous stable flight when its morphology is changed, the first two traverse the gaps passively. The works in [4], [5] propose the "transformable multirotor" and the "aerial robot dragon", respectively.

All the authors are with the Robotics and Perception Group, Dep. of Informatics, University of Zurich, and Dep. of Neuroinformatics, University of Zurich and ETH Zurich, 8050 Zurich, Switzerland.



(a) X configuration: no overlap. (b) O configuration: overlap.

(c) Hovering in O configuration without compensation. (d) Hovering in O configuration with compensation.

Fig. 1: Images of the foldable drone [1]. Top Left: the canonical configuration of the foldable drone i.e. the X configuration (a). Top right: the most compact configuration of the morphing platform i.e. the O configuration (b). Close-up views: experiments showing the transition in hovering from X to O configuration with compensation (d) and without compensation (c).

The former design was mainly conceived to grasp objects, whereas the latter requires a large space before and after the traversal of both vertical and horizontal gaps. Moreover, both aerial vehicles are cumbersome and their complex maneuvers are time consuming. On the other hand, the foldable drone proposed in [1] provides a more versatile and flexible frame that can cross both vertical and horizontal gaps while being compact, and in stable flight in any configuration, even in asymmetric ones.¹

All aforementioned works ignore most of the thrust losses generated by the interaction between the propellers and the rest of the vehicle's body. Aerodynamic effects have been analyzed in literature only for fixed-shape quadrotors. In [10] the authors presented theoretical and experimental investiga-

¹https://youtu.be/jmKXCdEbF_E

tions of a Vertically Offset Overlapped Propulsion System (VOOPS) where only the overlap between two adjacent propellers was considered. The most beneficial amount of overlap between propellers was determined offline, and the partial overlap between a propeller and the central body of the drone was not analyzed. The work in [11] analyzed in simulation the aerodynamic interactions in fixed shape quadrotors showing the ubiquitous loss of thrust due to the overlap between the propellers and the arms of a quadcopter. These results agree with [12] and [13], where the efficiency of the system with different arms mounted beneath different propellers was analyzed. However, this phenomenon may be accentuated in a morphing frame according to the dimensions of the regions of high pressure. Indeed, these issues not only depend on the regions of high pressure that are generated whenever the blades of the propeller overlap with the arms of the drone, but also on the different types of occlusions which hinder the wake of the propeller. The consequent loss of thrust is always present in quadrotors with upward mounted propellers, whereas, as shown in [14], [12], quadcopters with downward mounted rotors are claimed to have better performance. Finally, in [15], [16], [17] the ground effect in multirotors was analyzed. This aerodynamic effect is present in all rotor-based aerial vehicles and consists of the increment of thrust generated by the rotors when flying close to the ground due to the interaction of the rotor airflow with the ground surface. Sanchez *et al.* [16] started from an analytical model of the ground effect in helicopters and analyzed what they called "the partial ground effect", a situation in which only one or some of the rotors of the multirotor (but not all) are under the ground effect. Their analysis did not consider the propeller-body overlap which may happen in case of close proximity between the rotors and the robotic arm beneath them. The work in [15] provided a nonlinear dynamic model of the rotocraft in ground effect using multiple ring sources. Nevertheless, this model seemed to provide a more accurate characterization of the ground effect only for very large propellers.

A. Contributions

In this paper, we model the aerodynamic effects due to the *partial overlap* between the propellers and the central body of a quadrotor and experimentally identify it. To this end, we model such an interaction through experiments where the airflow of the propeller is hindered by different 3D-printed occlusion-structures (cf. Fig. 2) resembling the scenario of the foldable drone when more compact configurations are assumed. As a particular case study, we consider the foldable drone proposed in [1] in its most compact shape, the "O" configuration (Fig. 5b), in which all the arms are folded around the central body of the drone. In this scenario, the drone experiences a sudden loss of thrust, which makes it deviate from the reference position. To counteract this issue, we first analyze experimentally the consequences that the partial overlap implies comparing the results to the nominal case, i.e. to the case of no occlusion underneath the propeller (e.g. the "X" configuration Fig. 5a). Secondly, we derive a

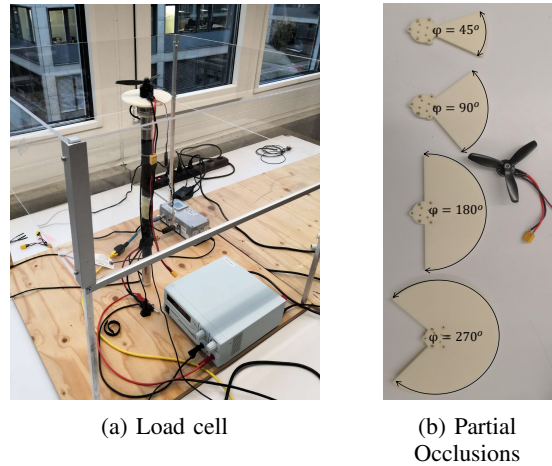


Fig. 2: Pictures of our experimental setup: (a) ATI Mini40 load cell and PSU that we used for all our measurements; (b) the 3D printed partial occlusions which replicate the foldable drone scenario.

novel geometry-aware formulation to compensate for these effects which does not rely on the state information as in [4], [5] and allows fast changes in configuration, more robust and stable control, and safer task completion. This formulation makes the vehicle aware of its geometry and able to estimate the occlusions below the propellers online. Finally, we deploy our geometry-aware compensation scheme based on the results of our performance analysis and characterization of the foldable drone, and evaluate the quality of these results to the position tracking in [1].

B. Structure of the Paper

In the following, we give an overview of the organization of the paper. In Sec. II, we present the experiments regarding the partial overlap. In Sec. III, we reveal the novel formulation of the geometry-aware compensation scheme. In Sec. IV, we demonstrate the effectiveness of our formulation against [1]. Finally, in Sec. VI and V, we illustrate the conclusions.

II. METHODOLOGY

In this section, we motivate our method, we illustrate the adopted experimental setup for the identification of our model, we provide a geometric description of the tested occlusions and we discuss the experimental results along with their physical implications.

A. Motivation

We propose a simple, yet effective, identification for our model which leverages an experimental approach. Nevertheless, a more theoretical approach could be followed by, for example, analyzing the nonlinear aerodynamic effects generated by the interaction between the airflow of the propellers and the presence of different partial occlusions. Although the second method might lead to a more precise solution, its derivation would be not only unfeasible for a real-time

system, but it would also require an experimental parameter identification. The simplicity of our method allows for a more general formulation of the problem while achieving precise results and allowing real-time computation of the necessary parameters.

B. Model Formulation

The thrust T produced by a single propeller is given by [18] as:

$$T = \rho A C_t (R\omega)^2, \quad (1)$$

where ρ is the density of air, A is the area of the propeller disk, C_t is the coefficient of thrust, R is the radius of the propeller and ω is the angular velocity of the propeller. In this paper we will simplify this notation as follows:

$$T = K_T \omega^2 \quad (2)$$

where K_T is what we call the thrust coefficient and ω is the angular velocity of the propeller. This notation corresponds to what we define as the nominal case i.e. the case of no occlusions beneath the propeller. To take into account the presence of a partial occlusion beneath the rotor we reformulate Eq. 2 as:

$$T = k(\phi)\omega^2, \quad (3)$$

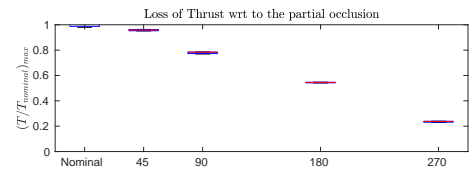
where ϕ is the angle which characterize the different partial occlusion and $k(\phi)$ is the related coefficient. We will refer to this coefficient as the *angle-dependent coefficient*. It is important to note that, in our notation, $k(\phi = 0^\circ)$ corresponds to K_T .

C. Experimental Setup for Parameters Identification

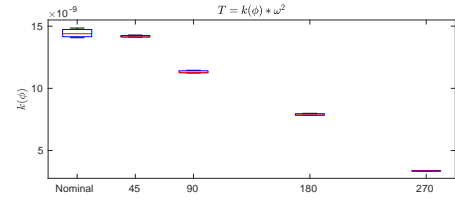
Our experimental setup consists of an ATI Mini40 load cell (Fig. 2a) which allows us to measure the thrust and the torque produced by the propeller with and without the presence of an occlusion beneath it. On top of the sensor, we mounted the occlusions depicted in Fig. 2b and the IQ2306 Speed Module 2200KV, an integrated motor and controller which provides feedback on the velocity of the rotor. Thanks to the feedback provided by the motor and the thrust measurements we can precisely determine the thrust coefficient of the propeller with different geometric occlusions and at different speeds. On top of the motor, we singularly tested 5 inches propellers (2 and 3 blades) and 6 inches propellers (2 and 3 blades).

In all the experiments, we provided a voltage of 12V to the motor through the PSU. To explore widely the trend of the thrust with different occlusions, we gave an input angular velocity to the motor consisting of 40 steps of 2 seconds each from a minimum of 100 *RPM* to a maximum of 19100 *RPM*. Due to physical limitations of the motor, an exception was made for the 3 blades, 6 inches propeller, in which case a maximum motor speed of 17188 *RPM* was provided.

In Fig. 2b, we show one of the novelties of this work, that is, the tested occlusions which partially hinder the airflow of the propeller to replicate the foldable drone scenario. They



(a) Thrust loss due to the partial occlusions (x-axis: ϕ)



(b) The angle dependent coefficient (x-axis: ϕ)

Fig. 3: Boxplot of 3 blades 5 inches propeller showing: (a) the loss of thrust with respect to the nominal case due to the partial occlusion; (b) the quadratic coefficient corresponding to the obtained reduced thrust. Both boxplots refer to the maximum value in our input 19100 *RPM*.

consist of different 3D printed sectors of a fix sized disk characterized by different angles $\phi \in \{45^\circ, 90^\circ, 180^\circ, 270^\circ\}$ which are designed to be mounted on top of the load cell and below the motor. In this paper, we will refer to these occlusions as *partial occlusions*.

D. Results of the Identification

For each partial occlusion, we observe how the thrust and the related thrust coefficient, at different motor speeds, change as a function of the angle of occlusion, namely as a function of ϕ . We consider the thrust loss to the nominal case, i.e. no occlusion, as a function of the angle of the partial occlusions ϕ . As expected, the loss of thrust is larger with a growing angle, that is, with bigger occlusions. Our experiments show that the thrust produced goes down linearly (Fig. 4). For the case of the 3 blades 5 inches propeller, that is the propeller that is mounted on the foldable drone, the produced thrust ranges from almost 90% to 25% of the nominal thrust with partial occlusions of $\phi = 45^\circ$ and $\phi = 270^\circ$ respectively. This is because the corresponding angle-dependent coefficient $k(\phi)$ of Eq. 3 follows the same trend (Fig. 3b). In Fig. 4 we can see the comparison between different propellers on the same occlusions. The general trend is repeated uniformly with opportune scale of the thrust due to the bigger or lower dimension of the propeller together with its number of blades.

However, the 2 blades propellers, lose more thrust than the 3 blades inches propellers. Despite 2 blades propellers are more efficient than 3 blades propellers, the last two produce more thrust than the first two if the partial occlusion is big enough ($\phi > 45^\circ$) (Fig. 4a). Indeed, the more thrust a rotor produces, the bigger the occlusion needs to be to hinder the propeller in the analysis. In Fig. 4b, a correlation between the angle-dependent coefficient of different propellers can be

deducted for big enough partial occlusions. For the case of propellers that have the same diameter, but different number of blades, the slopes of the angle dependent coefficients can be considered to be the same, whereas the vertical offset between the two lines increases with the dimension of the propeller, 0.5×10^{-8} between the 6 inches propellers and 0.4×10^{-8} between the 5 inches propellers. Moreover, for the case of propellers with different dimensions, but the same number of blades, the value of the angle-dependent coefficient doubles if the difference between their diameters is 1 inch. These experiments allow us to generalize the estimation of the angle-dependent coefficient to a broad variety of morphing and non-morphing aerial vehicles with different propellers. It is important to note that, in the foldable drone scenario, a bigger occlusion corresponds to a larger overlap between the propellers and the central body of the drone. Moreover, for the case of our morphing quadrotor, partial occlusions with $\phi > 65^\circ$ are not present due to the mechanical design of our platform.

Since all the measurements are assumed to be affected by white noise, we counteract this issue with averaging. For the implementation of our geometry-aware compensation scheme, we repeated each measurement three times and took the average of these three repetitions. The consequences of this operation are a more reliable approximation of the measurements with high variance and a more reliable compensation scheme.

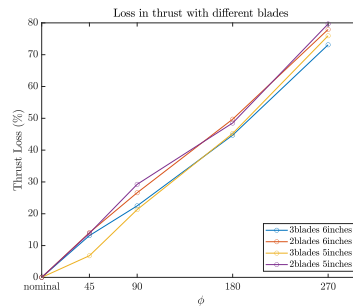
III. GEOMETRY-AWARE COMPENSATION SCHEME

In this section we provide the assumptions and the model approximations upon which our compensation scheme is based on along with its formulation.

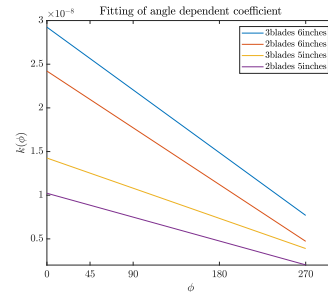
A. Assumptions

Because, for the case of the foldable drone, the overlap between propellers is less than 25% (for example in "H" and "T" configurations), as suggested in [10], the consequent loss of thrust is less than 5%, and hence negligible. In [1] the loss of thrust starts to be relevant whenever an overlap between the propellers and the central body of the vehicle occurs, due to the formation of a region of high pressure. Furthermore, the geometry-aware compensation scheme assumes that the main contribution of the thrust is near the tips of the rotor due to the high velocity airflow [11].

To estimate geometrically the partial occlusions, we simplified the quadrotor as follows (Fig. 5a): the central body of the drone is considered to be a square and the arms to be 4 dimension-less lines. We denote the angles of the arms with respect to the central body as θ_i while we denote the angles that characterize the partial occlusions as ϕ_i where $i \in \{1, 2, 3, 4\}$. Each arm is able to rotate in the following range $\theta_i \in [-\frac{\pi}{2}; \pi]$. In this work we will refer to ϕ_i as the angle of occlusion. It is important to note that the angle of occlusion can be computed at each time the drone decides to change its shape while flying by only knowing θ_i , and the geometry of the vehicle. Moreover, if there is no overlap



(a) Thrust loss percentage for different propellers.



(b) The angle dependent thrust coefficient for different propellers.

Fig. 4: Plot highlighting the comparison between different propellers: (a) the loss of thrust with respect to the nominal case due to the partial occlusion (all tested propellers); (b) the angle dependent coefficients of all the tested propellers. Both plots refer to the input 17188 RPM.

between the propellers and the central body of the drone, the thrust mapping remains unchanged.

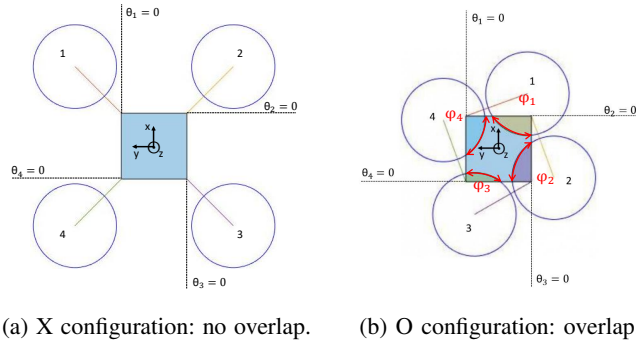
B. Formulation of the Compensation Scheme

The geometry-aware compensation scheme aims to modify the motor speeds of the foldable drone to overcome the effect of overlap while maintaining the same desired thrust of the previous configuration. To avoid the loss of thrust due to the overlap between the propellers and the central body of the drone, the angular velocities of the rotors must increase. To this end, we propose the following formulation:

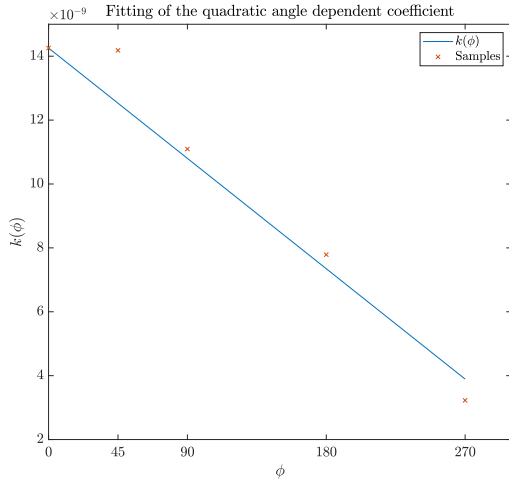
$$\hat{\omega} = \sqrt{\frac{\mathbf{T}}{K_T \mathbf{k}}}, \quad (4)$$

$$\mathbf{k} = \mathbf{1} - \frac{|K_T - \mathbf{k}(\phi)|}{K_T} \quad (5)$$

where $\hat{\omega} \in \mathbb{R}^4$ is the modified desired motors speeds which counteract the loss of thrust, $\mathbf{T} \in \mathbb{R}^4$ is the thrust that we want to produce, and $\mathbf{k} \in \mathbb{R}^4$ is a scaling factor which depends on the angle dependent coefficient $\mathbf{k}(\phi) \in \mathbb{R}^4$, and on what we called the thrust coefficient $K_T \in \mathbb{R}$. From our experimental data in Sec. II, knowing by visual inspection that the trend of the angle dependent coefficient as a function of different partial occlusions is linear with respect to their



(a) X configuration: no overlap. (b) O configuration: overlap.



(c) Fitting of the angle dependent coefficient.

Fig. 5: Images showing the default configuration of the foldable drone (a) and its most compact configuration (b) highlighting the angle of overlap between the propellers and the central body of the drone. On the bottom the fitting of the angle dependent coefficient on our experimental data obtained in Sec.II.

angles, we can fit a line to our data with the least squares method (Fig. 5c).

Once we geometrically derive ϕ , that is, the angle of occlusion of all the overlapped propellers, we are able to determine their corresponding angle dependent coefficients. The subtraction in Eq. 5 is related to the fact that the thrust decreases as the occlusions increase. Hence, the i^{th} scaling factor $k_i \in [0, 1]$ needs to be smaller than one to increase the angular velocity of the i^{th} propeller ω_i . From the formulation in Eq. 4, it derives that the amount of angular velocity needed to overcome the effect of the occlusion is $100\sqrt{\frac{1}{k_i}}$. Indeed, if $k_i(\phi) = 0$ then $k_i = 0$, which means that the occlusion is infinitely big and that the rotors must spin infinitely fast to overcome the effect generated by such occlusions. On the other hand, if $k_i(\phi) = K_T$ then $k_i = 1$, which means that there is no occlusion (e.g. Fig. 5a) and consequently that the rotors can spin as fast as before. Nevertheless, the motor might saturate in trying to overcome the loss of thrust introduced by the presence of a very big occlusion. In [1], this problem is already taken into account. The authors apply

the saturation scheme for the rotor thrusts proposed in [19], which prioritizes between the desired collective thrust and body torques according to their relevance for stabilizing the quadrotor and following a trajectory. Finally, it is important to note that, our geometric-aware compensation scheme is able to handle also non symmetric configurations of the foldable drone since it computes the angle dependent coefficient for each propeller independently. The computation of the angles of occlusion, and their corresponding angle dependent coefficients, is performed only when a specific geometric condition, that checks the overlap between a propeller and the central body of the quadcopter, is satisfied.

IV. DEPLOYMENT AND RESULTS

In this section, we present and discuss the performance of our proposed compensation scheme. We deployed our scheme on the foldable drone [1] and analyzed the performance of the quadrotor in nine experiments during both hovering and forward flight with vision based navigation.

Hovering - The drone hovers in X configuration, which represents the canonical configuration. The robot changes its shape during hovering from X to O configuration which is the most compact one and the most affected by the loss of thrust due to overlap between the propellers and the central body of the drone. When the drone ends the transition and reaches stable hovering it goes back to the X configuration. We performed the aforementioned experiments with both activated and deactivated compensation scheme. Finally, the morphing quadrotor always hovers in O configuration while at the same time switching on and off the compensation scheme.

Forward Flight - The drone follows a circular trajectory at a speed of 0.6 m/s on a circle of radius 1.5 m, at a constant height of 1.5 m. The robot changes its shape during flight switching between the X and O configurations with and without the activation of the compensation scheme. Finally, the foldable drone flies always in O configuration while at the same time switching on and off the compensation scheme. The same aforementioned experiments are then performed with the drone following a circular trajectory at a speed of 0.6 m/s on a circle of radius 1.5 m, but this time with a varying height that ranges from a minimum of 1.25 m to a maximum of 1.75 m. Fig. 6 and 7 show some quantitative results that prove the effectiveness of our proposed compensation.

A. Results

The compensation scheme improves the position tracking both in hovering and forward flight when the most compact configuration (i.e., O) is assumed. If the drone always hovers in X configuration the position errors are below 3.5 cm. When the drone switches to the O configuration and no compensation is provided, the quadrotor drifts more than 10 cm away from the desired position along all directions.

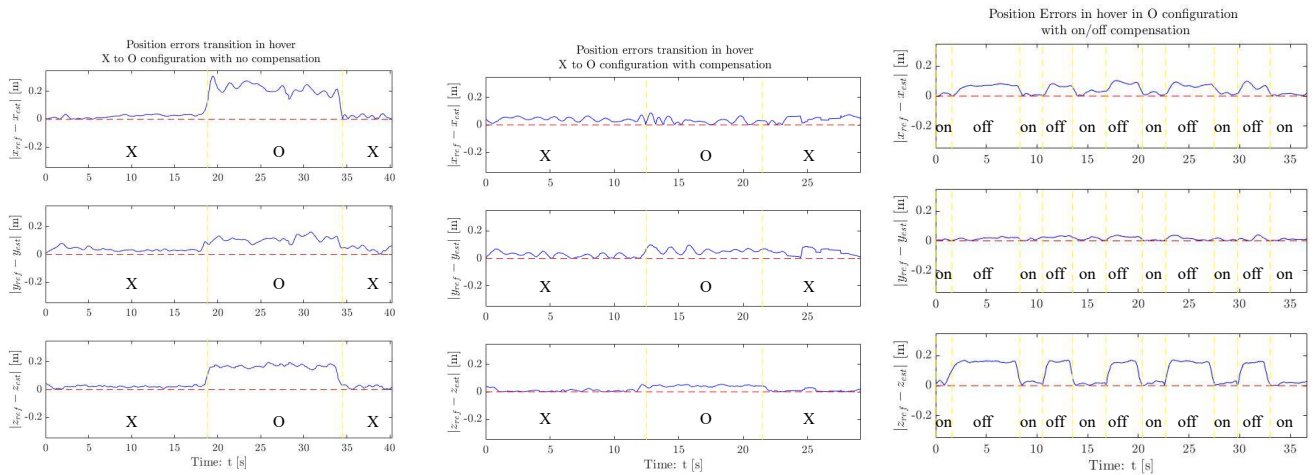


Fig. 6: Plots of the position error for the experimental validation of our geometry-aware compensation scheme. Left: transition in hovering from X to O configuration without compensation. Center: transition in hovering from X to O configuration with compensation. Right: hovering in O configuration switching on and off the compensation. Each row corresponds to a different axis of the world frame.

Experiments: Transitions in Hovering				
Start config	Final config	Position errors in final config [m]		
		$ x_r - x_e $	$ y_r - y_e $	$ z_r - z_e $
X	X	0.0336	0.0185	0.0142
X	O _{n.c.}	0.22	0.11	0.17
X	O _{c.}	0.030	0.044	0.043
O _{n.c.}	X	0.040	0.049	0.031
O _{c.}	X	0.047	0.042	0.00855
O _{c.}	O _{n.c.}	0.0748	0.0222	0.1594
O _{n.c.}	O _{c.}	0.0101	0.0003	0.0106

TABLE I: Hovering Performance. Position errors of the foldable drone computed as the absolute difference between the reference state (desired state) and the state estimate (approximation of the actual state) of the vehicle. The errors refer to the final configuration of the transition in hovering. In bold the best results, "c." stands for compensation and, "n.c." stands for no compensation.

For instance, the drone drops down of approximately 17 cm below the reference state and shifts 21 cm and 11 cm away from it along the x-axis and y-axis respectively (Tab. I). This drop (Fig. 1c) is due to the loss of thrust generated by the overlap between the propellers and the central body of the foldable drone. The experiments highlight also a translation along the x and y directions.

On one hand, this translation derives from the induced motion given by the rotation of arms while the drone drops and the turbulent flows generated by the overlaps. On the other hand, it is mainly due to the fact that all the arms are not rotated by the same angle (Fig. 5b). Indeed, arm 3 is less rotated than the other arms and, consequently, propeller 3 overlaps less with the central body. This is due to a geometric constraint related to the location of the battery

on the foldable drone. This means that propellers 1, 2, and 4 experience a stronger loss of thrust than propeller 3. This difference of thrusts makes the drone pitch and translate along the x -axis (21 cm away from the reference state) and slightly roll and translate along the y -axis (11 cm away from the reference state). The same transition in hovering from X to O configuration is much more stable when the compensation scheme is activated. Thanks to the integration of our geometry-aware compensation scheme, the position errors in O configuration are really close to the ones in the X configuration (all below 4.5 cm). Finally, when the drone switches back to X configuration, the desired state is reached with almost the same errors as before. This is the only case where the compensation scheme does not improve significantly the position tracking of the drone apart from the error along the z -axis.

The last experiment in hovering does not comprehend any changes in the shape of the drone during flight. The foldable drone always hovers in the O configuration. During flight, we switch on and off the compensation scheme to demonstrate how the aerodynamic effect of the overlap is ignored if this is deactivated. When the compensation is activated, the position errors are again drastically reduced, whereas, when the compensation scheme is switched off, the opposite occurs. In this case the biggest difference in position errors is along the z -axis since no change in configuration takes place and consequently no induced motion is produced.

Our compensation scheme boosted the performance of the morphing frame also in forward flight almost halving the euclidean distance between the reference trajectory and the actual one (Tab. 7). The activation of the compensation scheme allows the drone to immediately compensate for the aerodynamic effect regardless of what the previous configuration was, and without losing the track of the trajectory or

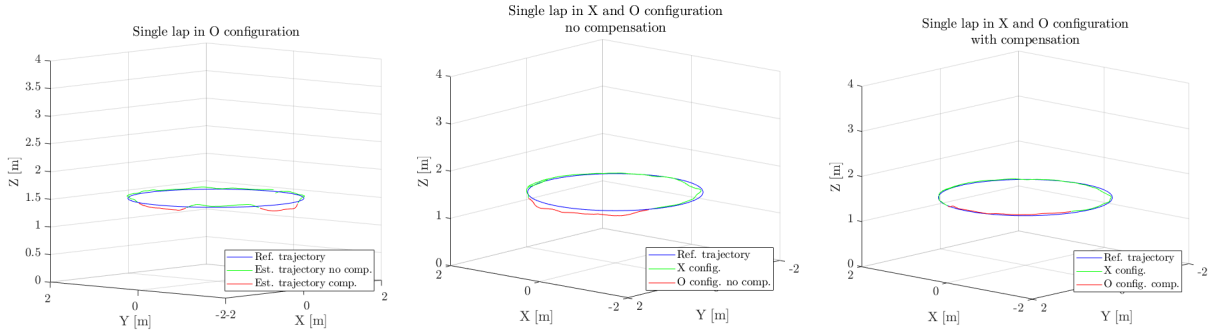


Fig. 7: 3D Plots of the circle trajectories at constant height flown by the foldable drone. The blue circles represent the reference trajectories. Left: in red O configuration without compensation; in green O configuration with compensation. Center: in red O configuration without compensation; in green X configuration. Right: in red O configuration with compensation; in green X configuration.

Experiments: Transitions in Hovering				
Start config	Final config	$\ddot{e} = k_P e + k_D \dot{e}$		
		\ddot{e} [m/s^2]	e [m]	\dot{e} [m/s]
X	$O_{n.c.}$	-0.50052	0.16859	-0.50489
X	$O_c.$	-0.03259	-0.0434	0.10318

TABLE II: Errors contribution to the PD controller for the gravity compensation. We define $e := z_{ref} - z_{est}$. Note: "c." stands for compensation and, "n.c." stands for no compensation.

deviate from it significantly.

To further understand the impact of our proposed compensation scheme, we compute its contribution to the already present PD controller for the gravity compensation (Tab. II). When the foldable drone is in hovering, the total acceleration should be equal to gravity. If the compensation is not activated, gravity acceleration is reached with a strong contribution of the position error. However, when the compensation is used, the opposite occurs. This thrust mapping reduces significantly such position error from 0.16859 to -0.0434 to maintain the position. Consequently, the compensation scheme provides a better feed-forward term which leads to a smaller effort requested by the PD controller. Our model reduced the position errors along all directions when the most compact configuration of the foldable drone is assumed and its deployment provided a better trajectory tracking for the morphing platform. The correct thrust mapping is now recovered, and a more stable and robust flight can be achieved.

V. DISCUSSION

The role of morphing drones is always increasing for their versatile structure to perform specific tasks. Consequently, the need of thrust mapping of this kind will be increasingly requested, not only by different types of morphing quadrotors, but also by drones that carry changing loads or a robotic arm.

Experiments: Statistics Transitions in Forward Flight [m]						
Morphology Transitions	μ_X	σ_X	$\mu_{O_{n.c.}}$	$\sigma_{O_{n.c.}}$	$\mu_{O_c.}$	$\sigma_{O_c.}$
X - $O_{n.c.}$	0.0772	0.0414	0.2172	0.0787	-	-
$O_{n.c.}$ - $O_c.$	-	-	0.2339	0.050	0.1210	0.045
X - $O_c.$	0.0898	0.0452	-	-	0.1389	0.0482
X - $O_{n.c.}$	0.1211	0.0426	0.2690	0.0681	-	-
$O_{n.c.}$ - $O_c.$	-	-	0.2134	0.0452	0.1318	0.0611
X - $O_c.$	0.0975	0.0363	-	-	0.1038	0.0439

TABLE III: Flight performance. Statistics for the position error in forward flight for the canonical and most compact morphologies. Mean μ and standard deviation σ for the euclidean distance in meters between the estimated position and the reference state. The first block considers flight in a circle with constant height, the second block concerns flight in a circle with varying height. Note: "c." stands for compensation and, "n.c." stands for no compensation.

The presented compensation scheme for the specific platform of the foldable drone can be extended to any multirotors (fixed or morphing) whenever the analyzed geometric occlusions are present on the vehicle. An alternative approach to tackle these problems could have involved the addition of an integral action on the already existing controller. However, we claim that the proposed novel approach has multiple advantages. The integral action can bring precision to slow systems, but when the imposed value varies rapidly and significantly, the integrator slows down the whole system, producing very often oscillations. Moreover, the integral action is effective only with a constant reference (in hovering), whereas, for the case of a time varying set-point, this effectiveness is almost lost. In addition to this limitation, the integrator also depends on the error of the state. Consequently, the integral action would start to have an impact only after the aerodynamic effect in analysis has affected the closed-loop system. However, our proposed geometry-aware compensation scheme does not suffer from these issues. It maintains the same power consumption as in [1] without affecting the velocity of the transition among

different morphologies, and continuously compensating for the loss of thrust with respect to the dimension of the occlusions beneath the propellers. Finally, the proposed method exploits the actual physics of the phenomenon, without relying on any information of the state and without the tuning of any parameters. The action in feed-forward of our compensation scheme is able to overcome the loss of thrust immediately and the application of this compensation scheme only requires the knowledge of the geometry of the vehicle and the presence of the analyzed occlusions.

VI. CONCLUSION

In this work, we presented, for the first time, a simple, yet effective analysis of the interaction between a single propeller and different partial occlusions. We leveraged this analysis to propose the novel geometry-aware compensation scheme. We proved its effectiveness by deploying it on the foldable drone and testing it both in hovering and forward flight. Our model improved the position tracking of the foldable drone in the configuration where its performance was affected the most (i.e., O configuration), reaching almost the desired position and achieving more reliable, safe, and accurate flight.

Our work achieved a reduction of the position errors up to 20 cm in hovering, doubled the tracking accuracy of the drone in forward flight in the O configuration and, at the same time, reducing the effort of the PD controller, without additional power consumption and without increasing the execution time of the task that the drone is performing. Given the presence of the analyzed occlusions, our work can be extended to any multirotor aerial vehicle with either fixed or changing shape.

REFERENCES

- [1] D. Falanga, K. Kleber, S. Mintchev, D. Floreano, and D. Scaramuzza, "The foldable drone: A morphing quadrotor that can squeeze and fly," *IEEE Robotics and Automation Letters*, pp. 209–216, 2018.
- [2] V. Riviere, A. Manecy, and S. Viollet, "Agile robotic fliers: A morphing-based approach," *Soft robotics*, pp. 541–553, 2018.
- [3] Y. Bai and S. Gururajan, "Evaluation of a baseline controller for autonomous "figure-8" flights of a morphing geometry quadcopter: Flight performance," *Drones*, p. 70, 2019.
- [4] M. Zhao, K. Kawasaki, X. Chen, S. Noda, K. Okada, and M. Inaba, "Whole-body aerial manipulation by transformable multirotor with two-dimensional multilinks," in *2017 IEEE International Conference on Robotics and Automation (ICRA)*. IEEE, 2017, pp. 5175–5182.
- [5] M. Zhao, T. Anzai, F. Shi, X. Chen, K. Okada, and M. Inaba, "Design, modeling, and control of an aerial robot dragon: A dual-rotor-embedded multilink robot with the ability of multi-degree-of-freedom aerial transformation," *IEEE Robotics and Automation Letters*, pp. 1176–1183, 2018.
- [6] N. Bucki and M. W. Mueller, "Design and control of a passively morphing quadcopter," in *2019 International Conference on Robotics and Automation (ICRA)*. IEEE, 2019, pp. 9116–9122.
- [7] A. Otto, N. Agatz, J. Campbell, B. Golden, and E. Pesch, "Optimization approaches for civil applications of unmanned aerial vehicles (uavs) or aerial drones: A survey," *Networks*, vol. 72, no. 4, pp. 411–458, 2018.
- [8] J. Delmerico, S. Mintchev, A. Giusti, B. Gromov, K. Melo, T. Horvat, C. Cadena, M. Hutter, A. Ijspeert, D. Floreano *et al.*, "The current state and future outlook of rescue robotics," *Journal of Field Robotics*, vol. 36, no. 7, pp. 1171–1191, 2019.

- [9] H. Shakhatreh, A. H. Sawalmeh, A. Al-Fuqaha, Z. Dou, E. Almaita, I. Khalil, N. S. Othman, A. Khreishah, and M. Guizani, "Unmanned aerial vehicles (uavs): A survey on civil applications and key research challenges," *IEEE Access*, vol. 7, pp. 48 572–48 634, 2019.
- [10] G. Nandakumar, A. Srinivasan, and A. Thondiyath, "Theoretical and experimental investigations on the effect of overlap and offset on the design of a novel quadrotor configuration, voops," *Journal of Intelligent & Robotic Systems*, pp. 615–628, 2018.
- [11] S. Yoon, P. V. Diaz, D. D. Boyd Jr, W. M. Chan, and C. R. Theodore, "Computational aerodynamic modeling of small quadcopter vehicles," in *American Helicopter Society (AHS) 73rd Annual Forum Fort Worth, Texas*, 2017.
- [12] B. Theys, G. Dimitriadis, P. Hendrick, and J. De Schutter, "Influence of propeller configuration on propulsion system efficiency of multi-rotor unmanned aerial vehicles," in *2016 international conference on unmanned aircraft systems (ICUAS)*. IEEE, 2016, pp. 195–201.
- [13] N. Fernandes, "Design and construction of a multi-rotor with various degrees of freedom," *Universidade Técnica de Lisboa, Lisboa*, 2011.
- [14] P. Pounds, R. Mahony, J. Gresham, P. Corke, and J. M. Roberts, "Towards dynamically-favourable quad-rotor aerial robots," in *Proceedings of the 2004 Australasian Conference on Robotics & Automation*. Australian Robotics & Automation Association, 2004.
- [15] C. G. Hooi, F. D. Lagor, and D. A. Paley, "Flow sensing, estimation and control for rotorcraft in ground effect," in *2015 IEEE Aerospace Conference*. IEEE, 2015, pp. 1–8.
- [16] P. Sanchez-Cuevas, G. Heredia, and A. Ollero, "Characterization of the aerodynamic ground effect and its influence in multirotor control," *International Journal of Aerospace Engineering*, 2017.
- [17] D. D. C. Bernard, F. Riccardi, M. Giurato, and M. Lovera, "A dynamic analysis of ground effect for a quadrotor platform," *IFAC-PapersOnLine*, vol. 50, no. 1, pp. 10 311–10 316, 2017.
- [18] G. Leishman, *Principles of helicopter aerodynamics*. Cambridge University Press, 2002.
- [19] M. Faessler, D. Falanga, and D. Scaramuzza, "Thrust mixing, saturation, and body-rate control for accurate aggressive quadrotor flight," *IEEE Robotics and Automation Letters*, vol. 2, no. 2, pp. 476–482, 2016.